Baade's window and APOGEE

Metallicities, ages, and chemical abundances

M. Schultheis[1], A. Rojas-Arriagada[1,22,3], A. E. García Pérez[4,5], H. Jönsson[4,5], M. Hayden[1], G. Nandakumar[1],
K. Cunha[6], C. Allende Prieto[4,5], J. A. Holtzman[7], T. C. Beers[8], D. Bizyaev[9,10], J. Brinkmann[9], R. Carrera[4],
R. E. Cohen[11], D. Geisler[11], F. R. Hearty[12], J. G. Fernandez-Tricado[13], C. Maraston[14], D. Minnitti[2,3,15],
C. Nitschelm[16], A. Roman-Lopes[17], D. P. Schneider[12,18], B. Tang[11], S. Villanova[11],
G. Zasowski[19,20], and S. R. Majewski[21]

[1] Laboratoire Lagrange, Université Côte d'Azur, Observatoire de la Côte d'Azur, CNRS, Bd de l'Observatoire, 06304 Nice, France
e-mail: mathias.schultheis@oca.eu
[2] Departamento de Fisica, Facultad de Ciencias Exactas, Universidad Andres Bello Av. Fernandez Concha 700,
7591538 Las Condes, Santiago, Chile
[3] Millennium Institute of Astrophysics, Av. Vicuña Mackenna 4860, 782-0436 Macul, Santiago, Chile
[4] Instituto de Astrofísica de Canarias (IAC), 38205 La Laguna, Tenerife, Spain
[5] Universidad de La Laguna, Dpto. Astrofísica, 38206 La Laguna, Tenerife, Spain
[6] Observatório Nacional, 20921-400 Sao Cristóvao, Rio de Janeiro, Brazil
[7] New Mexico State University, Las Cruces, NM 88003, USA
[8] Department of Physics and JINA Center for the Evolution of the Elements, Univ. of Notre Dame, Notre Dame, IN 46556, USA
[9] Apache Point Observatory and New Mexico State University, PO Box 59, Sunspot, NM 88349-0059, USA
[10] Sternberg Astronomical Institute, Moscow State University, 119991 Moscow, Russia
[11] Departamento de Astronomía, Casilla 160-C, Universidad de Concepción, Concepción, Chile
[12] Department of Astronomy and Astrophysics, The Pennyvania State University, University Park, PA 16802, USA
[13] The Observatoire des sciences de l'Univers de Besançon, 41 avenue de l'Observatoire, 25000 Besançon, France
[14] ICG-University of Portsmouth, Dennis Sciama Building, Burnaby Rd., Portsmouth, PO13FX, UK
[15] Vatican Observatory, V00120 Vatican City State, Italy
[16] Unidad de Astronomía, Universidad de Antofagasta, Avenida Angamos 601, 1270300 Antofagasta, Chile
[17] Departamento de Física, Facultad de Ciencias, Universidad de La Serena, Cisternas 1200, La Serena, Chile
[18] Institute for Gravitation and the Cosmos, The Pennsylvania State University, University Park, PA 16802, USA
[19] Center for Astrophysical Sciences, Department of Physics and Astronomy, Johns Hopkins University, 3400 North Charles Street,
Baltimore, MD 21218, USA
[20] Department of Physics & Astronomy, University of Utah, 115 S. 1400 E., Salt Lake City, UT 84112, USA
[21] Department of Astronomy, University of Virginia, Charlottesville, VA 22904, USA
[22] Instituto de Astrofísica, Facultad de Física, Pontificia Universidad Católica de Chile, Av. Vicuña Mackenna 4860, Santiago, Chile

ABSTRACT

Context. Baade's window (BW) is one of the most observed Galactic bulge fields in terms of chemical abundances. Owing to its low and homogeneous interstellar absorption it is considered the perfect calibration field for Galactic bulge studies.
Aims. In the era of large spectroscopic surveys, calibration fields such as BW are necessary for cross calibrating the stellar parameters and individual abundances of the APOGEE survey.
Methods. We use the APOGEE BW stars to derive the metallicity distribution function (MDF) and individual abundances for α- and iron-peak elements of the APOGEE ASPCAP pipeline (DR13), as well as the age distribution for stars in BW.
Results. We determine the MDF of APOGEE stars in BW and find a remarkable agreement with that of the *Gaia*-ESO survey (GES). Both exhibit a clear bimodal distribution. We also find that the Mg-metallicity planes of the two surveys agree well, except for the metal-rich part ([Fe/H] > 0.1), where APOGEE finds systematically higher Mg abundances with respect to the GES. The ages based on the [C/N] ratio reveal a bimodal age distribution, with a major old population at ∼10 Gyr, with a decreasing tail towards younger stars. A comparison of stellar parameters determined by APOGEE and those determined by other sources reveals detectable systematic offsets, in particular for spectroscopic surface gravity estimates. In general, we find a good agreement between individual abundances of O, Na, Mg, Al, Si, K, Ca, Cr, Mn, Co, and Ni from APOGEE with that of literature values.
Conclusions. We have shown that in general APOGEE data show a good agreement in terms of MDF and individual chemical abundances with respect to literature works. Using the [C/N] ratio we found a significant fraction of young stars in BW.

Key words. Galaxy: bulge – Galaxy: stellar content – stars: fundamental parameters – stars: abundances – infrared: stars

1. Introduction

Large high-resolution spectroscopic surveys in the Galactic bulge such as APOGEE (Majewski et al. 2015), *Gaia*-ESO (GES, Gilmore et al. 2012), or ARGOS (Ness et al. 2013) may suffer from systematic biases in terms of stellar parameters or individual abundances. In the case of APOGEE, Baade's window (BW) was chosen to validate stellar parameters and

chemical abundances with known previous measurements in the literature for high metallicities. Owing to its low and homogeneous interstellar extinction (see e.g. Stanek 1996; Gonzalez et al. 2011b), BW is an ideal field in the Galactic bulge for validation purposes. It also has the advantage of covering a wide range of metallicities.

The era of chemical-abundance studies of the Galactic bulge in BW started in the late 1980s with Rich (1988), who obtained metallicities and α-elements for 88 K giants. Rich (1988) found evidence for super metal-rich stars and derived a mean [Fe/H] = +0.2. McWilliam & Rich (1994) acquired high-resolution spectra ($R \sim 17\,000$) of 11 bulge K giants, and revised the abundance distribution in BW with a mean [Fe/H] = −0.25, and confirmed enhancements of the α-elements Mg and Ti, and of Al. From a much larger sample of K and M giants, Sadler et al. (1996) obtained a similar mean metallicity to the McWilliam & Rich (1994) values, but less enhanced in Mg. Adopting new abundance determination techniques and linelists, tailored to analyse metal-rich giants, Fulbright et al. (2006) analysed 27 K giants, and reported a mean metallicity comparable to that of the local disc. In addition, they found that the α-elements O, Mg, Si, Ca, and Ti, and the odd-Z elements Al and Na, are enhanced relative to the Galactic thin disc, indicating that massive stars contributed to the chemical enrichment of the bulge (Fulbright et al. 2007a). Zoccali et al. (2006) found, based on high-resolution UVES (ESO-VLT) spectra ($R = 47\,000$), enhanced O, Mg, and Al abundances (see also Lecureur et al. 2007). Contrary to these studies, Meléndez et al. (2008) did not identify any significant difference in the abundance patterns of C, N, and O between the thick disc and the Galactic bulge, suggesting that the bulge and the local thick disc experienced similar chemical evolution histories. Alves-Brito et al. (2010) confirmed this similarity by observing a Galactic bulge sample and a local thick disc sample.

With the advent of the FLAMES multiobject spectrograph at the VLT (Pasquini et al. 2003), it became possible to observe a large number of objects simultaneously at high spectral resolution, a sizable leap for this type of study. Hill et al. (2011) analysed approximately 200 FLAMES/GIRAFFE spectra ($R = 20\,000$) of red clump stars in BW, which revealed the presence of two populations in their metallicity distribution function (MDF): a metal-poor component centred on [Fe/H] = −0.30 and [Mg/H] = −0.06 with a large dispersion, and a narrow metal-rich component centred around [Fe/H] = +0.32 and [Mg/H] = +0.35. These two components also exhibit kinematical differences; the metal-poor component is compatible with an old spheroid, whereas the metal-rich component is consistent with a population supporting a bar (Babusiaux et al. 2010). Gonzalez et al. (2011a) analysed abundances of Mg, Si, Ca, and Ti for the Zoccali et al. (2008) sample, and concluded from their large sample of bulge stars that there is chemical similarity between the thick disc and the bulge. The GES observed several bulge fields including BW (Rojas-Arriagada et al. 2014), and they confirmed the bimodal nature of the MDF using Gaussian-mixture models (GMM). Zoccali et al. (2017) also obtained the bimodal MDF for a large number of bulge fields using the GIBS survey. In addition, they found that these two components have different spatial distributions; the metal-poor population is more centrally concentrated, while the metal-rich population exhibits a boxy concentration, as expected for a bar seen edge-on.

All of the studies mentioned above were based on spectroscopy in the visible wavelength range. With the development of near-IR detectors, Galactic bulge studies could begin to take advantage of the fact that the flux in the near-IR band is several magnitudes higher than in the visible for K/M giants,

and that the extinction in the infrared is much less severe (by roughly a factor of 10 in the K-band) compared to the visual. Rich & Origlia (2005) performed the first detailed abundance analysis of 14 M giants in BW, based on $R = 25\,000$ infrared spectra ($1.5-1.8\ \mu$m) using the NIRSPEC facility at the *Keck* telescope. They found very similar iron abundances to those of K giants, but α enhancements compared to a local disc sample of M giants. Cunha & Smith (2006) determined individual elemental-abundance estimates such as C, N, O, Na, Ti, and Fe for BW K/M giants. They found their stars to be enriched in O and in Ti, suggesting a rapid chemical enrichment of the Galactic bulge. Ryde et al. (2010) determined abundance ratios for 11 bulge giants, and found enhanced [O/Fe], [Si/Fe], and [S/Fe] ratios with increasing metallicity, up to approximately [Fe/H] $\sim$ −0.3. However, all of these studies were based on single-slit spectroscopy, leading to a limited number of objects. The APOGEE survey (Majewski et al. 2015) is the first large-scale near-IR, high-resolution ($R \sim 22\,500$) survey, with its 300 fibre spectrograph able to assemble, for the first time, large samples of bulge stars with this information.

Our aim in this paper is to compare stellar parameters and individual abundances, for α- and iron-peak elements, of the APOGEE ASPCAP pipeline (DR13) with respect to previously found literature values for stars in BW. We also compare the relative location of the bulge sequence in the [α/Fe] vs. [Fe/H] plane as seen by the APOGEE and GES surveys. The study of Galactic stellar populations is entering the era of big data. Surveys such as APOGEE and GES are producing massive internally homogeneous databases of parameters and abundance ratios for samples of several thousands of stars. In this context, it is of great importance to properly characterize the eventual scale differences between results provided by different surveys for stars in common.

2. The samples

2.1. APOGEE

The Apache Point Observatory Galactic Evolution Experiment (APOGEE; Majewski et al. 2015) began as one of four Sloan Digital Sky Survey-III (SDSS-III, Eisenstein et al. 2011) experiments. It is a large-scale, near-IR, high-resolution ($R \sim 22\,500$) spectroscopic survey of Milky Way stellar populations (Zasowski et al. 2013). The survey uses a dedicated, 300-fibre, cryogenic spectrograph coupled to the wide-field Sloan 2.5 m telescope (Gunn et al. 2006) at the Apache Point Observatory (APO). APOGEE observes in the H-band, ($1.5-1.7\ \mu$m), where extinction by dust is significantly lower than at optical wavelengths ($A_{\rm V}/A_{\rm H} = 6$). Stellar parameters and chemical abundances for up to 22 elements can be determined by the Apogee Stellar Parameters and Chemical Abundances Pipeline (ASPCAP, García Pérez et al. 2016). These values are based on a χ^2 minimization between observed and synthetic model spectra (see Zamora et al. 2015; Holtzman et al. 2015 for more details), performed with the FERRE code (Allende Prieto et al. 2006, and subsequent updates). Several improvements in the data processing and analysis as presented in Data Release 13 (DR13, SDSS Collaboration et al. 2016) have been accomplished; for example, the variation of the line-spread function (LSF) as a function of the fibre number has been taken into account. A new updated line list has been used to determine stellar parameters and abundances, and a new MARCS model atmosphere grid going down to $T_{\rm eff} < 3500$ K has been used as well. In addition, separate synthetic spectral grids are used for dwarfs and giants, and updated relationships for the
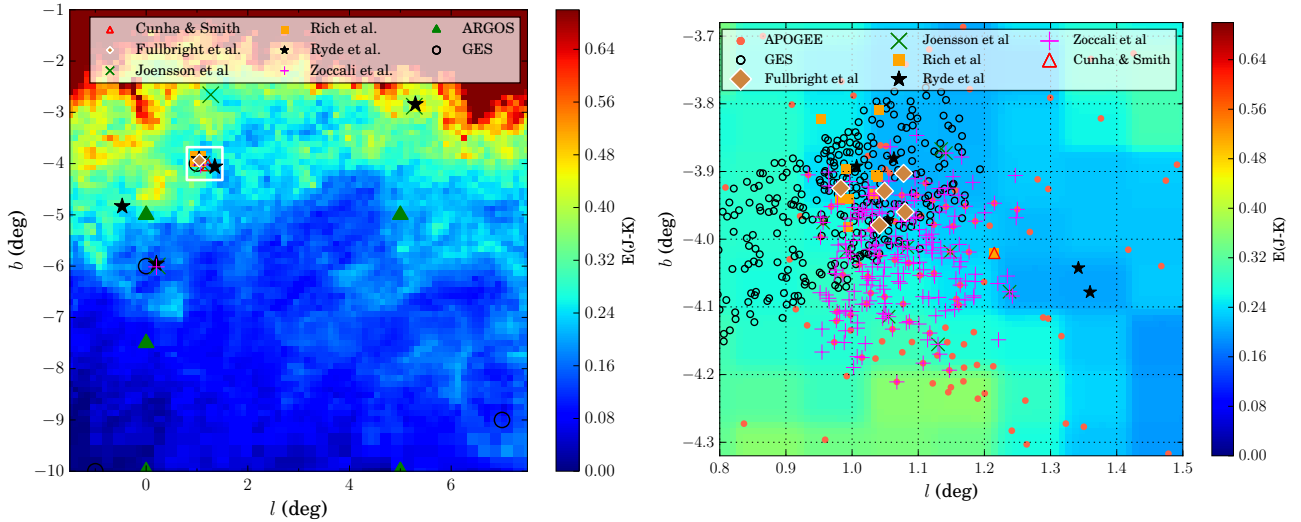
Fig. 1. Baade's window finding chart. *Left panel*: position of Baade's window in a broader bulge area depicted by an extinction map (white box), as obtained from the results of Gonzalez et al. (2012). The approximate position of other studied bulge fields, including those of the ARGOS and GES surveys, are depicted as indicated in the figure. *Right panel*: zoom of the highlighted area around Baade's window showing the position of individual stars from the studies compared to APOGEE in this paper. The distribution of APOGEE targets span a larger area, so that the targets displayed here are a subset of those adopted in this study.

micro-turbulence and macro-turbulence have been adopted. For more details we refer the interested reader to Holtzman et al. (in prep.) and the DR13 online documentation.

Baade's window has been observed in two Sloan fibre plug-plates (5817 and 5818), resulting in a total of 425 unique objects. A total of 287 stars were observed in the regular target selection mode of APOGEE (extratarget flag ==0) with the usual colour cut of $(J-K)_0 > 0.5$ (see Zasowski et al. 2013); in addition, 138 stars came from a commissioning plug-plate which have lower quality. For stellar parameter estimates we used the calibrated stellar parameters (PARAM) and individual chemical abundances ([X/Fe]), which were calibrated using a sample of well-studied field and cluster stars, including a large number of stars with asteroseismic stellar parameters from NASA's Kepler mission (see Holtzman et al. 2015 and in prep.). Using calibrated parameters implies a limit in $\log g < 3.8$. The abundances were calibrated internally, using data for stars in open clusters in an attempt to remove abundance trends with effective temperature. In addition, the abundances have now been calibrated externally in order to go through [X/Fe] = 0 at [Fe/H] = 0 for local thin disc stars.

In order to retrieve the stellar parameters and the chemical abundances of the Baade's window field, it is necessary to download the corresponding fits table file[1] where all relevant information such as stellar parameters ($T_{\rm eff}$, $\log g$, [Fe/H], [α/Fe]), chemical abundances, photometry, etc., are stored. The detailed description of this data file can be found on the corresponding webpage[2]. We note that both uncalibrated and calibrated stellar parameters, as well as chemical abundances, are given in this file. For BW, the easiest way to retrieve the 425 objects is to search for the field name "BAADEWIN". In the left panel of Fig. 1, the position of Baade's window is highlighted in a broader view of the bulge region. The background colour map depicts the reddening variations according to the results of Gonzalez et al. (2012).

---

[1] http://www.sdss.org/dr13/irspec/spectro_data/allStar-l30e.2.fits

[2] https://data.sdss.org/datamodel/files/APOGEE_REDUX/APRED_VERS/APSTAR_VERS/ASPCAP_VERS/RESULTS_VERS/allStar.html

The position of several fields studied in the literature, including the ARGOS and GES surveys, are depicted to put BW in the context of other bulge studies.

Figure 2 shows the 2MASS colour–magnitude diagram (H vs. $J-K$) for Baade's window. The APOGEE and DR1-GES samples are colour-coded as a function of metallicity. We also show the PARSEC isochrones (Bressan et al. 2012), assuming an age of 10 Gyr, with varying metallicities assuming that the stars in BW have a mean distance of 8.4 kpc (Chatzopoulos et al. 2015). We assume an average extinction of $A_{\rm V} = 1.5$ (Stanek 1996), and the reddening law of Nishiyama et al. (2009), which we used to redden the isochrones. Stars with $\log g > 3.5$ have been excluded. We see clearly that the APOGEE stars have redder $(J-K)_0$ colours than predicted by the most metal-rich isochrones ($Z = 0.07$). While the metal-poor stars generally have bluer $(J-K)$ colours, stars with similar spectroscopically determined metallicities show a wide range in the $(J-K)$ colour.

2.2. Comparison samples

As mentioned in Sect. 2.1, BW was targeted by APOGEE for calibration with respect to studies having well-established stellar parameters and chemical abundances. For the cross-identification of coordinates and 2MASS IDs of our stars, we used Table 1 of Church et al. (2011), who provided coordinates and 2MASS names for all stars in Arp's finding chart (Arp 1965). Fulbright et al. (2006) obtained effective temperatures based on $V-K$ data, together with the photometric transformation to $T_{\rm eff}$ from Alonso et al. (1999). In total we have five stars in common with Fulbright et al. (2006, hereafter Ful06), four stars with Rich & Origlia (2005, hereafter Rich05), three with Ryde et al. (2010, hereafter Ryde10), one with Cunha & Smith (2006, hereafter Cunha06), and 55 with Zoccali et al. (2008, hereafter Zocc08). The right panel of Fig. 1 displays the position of the individual stars in all these studies. The region displayed corresponds to that highlighted by a white square in the left panel of the same figure. Table 1 lists the stellar parameters of the different literature values, as well as those from APOGEE (DR13, SDSS Collaboration et al. 2016).

Table 1. Comparison of stellar parameters.

2MASSid	T_{eff}	$\log g$	[Fe/H]	Colour	$T_{\mathrm{eff}}^{\mathrm{APOGEE}}$	$\log g^{\mathrm{APOGEE}}$	[Fe/H]$^{\mathrm{APOGEE}}$	Ref.
18033576-2958353	4257	1.55	−0.37	2.929[a]	4179	1.79	−0.36	Ful06
18034989-3000083	4184	1.53	0.16	3.050[a]	4251	2.42	0.28	Ful06
18033819-3000515	4097	0.87	−1.15	3.269[a]	4411	2.07	−0.89	Ful06
18034938-3002440	4554	1.66	−1.22	2.552[a]	4392	1.52	−1.17	Ful06
18032824-3004108	4157	1.58	−0.41	3.124[a]	4090	1.78	−0.38	Ful06
18032356-3001588	3902	0.51	−1.25	3.776[b]	3994	1.40	−1.04	Ryde10
18032843-2958416	4197	1.29	−0.90	3.103[b]	4202	1.67	−0.85	Ryde10
18034939-3001541	4106	0.89	−0.23	3.131[b]	4194	1.86	−0.08	Ryde10
18042265-2954518	3200	0.50	−0.15	1.370[b]	2994	−0.06	−0.16	Rich05
18042265-2954518	3375	0.40	−0.05	1.370[b]	2994	−0.06	−0.16	Cunha06
18030810-2957480	3200	0.50	−0.17	1.300[b]	3080	−0.23	−0.49	Rich05
18033169-3000437	4000	1.00	−0.09	0.840[b]	3767	1.24	−0.21	Rich05
18033374-3003572	4000	1.00	−0.03	0.840[b]	3853	1.25	−0.29	Rich05
18034320-2959404	4850	1.93	−0.37	1.667[c]	4298	1.78	−0.76	Zocc08
18034616-2958303	4000	1.52	0.51	2.083[c]	4124	2.21	0.38	Zocc08
18040747-2955001	4250	1.70	0.05	2.050[c]	4128	2.10	0.20	Zocc08
18040026-2958253	4850	2.00	−0.67	1.690[c]	4398	1.87	−0.94	Zocc08
18041720-2956497	4400	1.84	−0.05	2.081[c]	4156	1.83	−0.18	Zocc08
18043406-2959546	4930	2.04	−0.10	1.636[c]	4207	2.43	0.11	Zocc08
18042724-3001108	5100	2.06	−0.22	1.527[c]	3270	−0.37	−2.15	Zocc08
18042722-2958570	4700	1.94	−0.20	1.793[c]	4327	2.19	−0.42	Zocc08
18040883-3002037	4200	1.67	−0.24	2.036[c]	4092	1.83	−0.26	Zocc08
18041554-3001431	4550	1.81	−0.45	1.814[c]	4210	1.80	−0.63	Zocc08
18041486-3010159	4850	2.12	0.45	1.700[c]	3810	1.86	0.34	Zocc08
18041410-3007315	4550	1.87	−0.04	1.925[c]	4193	2.15	−0.25	Zocc08
18035937-3006027	4500	1.91	−0.60	1.931[c]	4172	2.09	−0.64	Zocc08
18033691-3007047	4600	1.97	0.05	2.017[c]	4157	1.90	−0.21	Zocc08
18041187-3006214	4300	1.74	−0.22	2.072[c]	4109	1.83	−0.29	Zocc08
18041606-3005254	4200	1.67	0.40	2.029[c]	4229	2.28	0.37	Zocc08
18033660-3002164	4950	2.00	−1.05	1.664[c]	4927	2.23	−1.12	Zocc08
18034092-3004423	4650	1.99	−0.21	1.858[c]	4313	2.78	−0.46	Zocc08
18034906-3003384	4500	1.87	−0.32	1.876[c]	4252	1.83	−0.49	Zocc08
18035632-2956410	4350	1.84	0.27	2.255[c]	4173	2.42	0.53	Zocc08
18035131-2957281	4400	1.91	−0.08	2.192[c]	4075	1.96	−0.14	Zocc08
18034379-2957162	4350	2.03	0.22	2.296[c]	3970	2.09	−0.36	Zocc08
18041178-2951100	4400	1.86	0.15	2.028[c]	4237	2.33	0.22	Zocc08
18040492-2952427	4400	1.91	0.29	2.133[c]	4232	2.48	0.20	Zocc08
18040398-2959223	4100	1.70	−0.15	2.255[c]	3857	1.09	−0.48	Zocc08
18035929-2949519	4150	1.87	0.28	2.520[c]	4011	1.78	0.33	Zocc08
18040008-2955079	4500	1.96	−0.05	2.077[c]	4165	2.17	−0.26	Zocc08
18041328-2958182	4300	1.87	0.25	2.192[c]	4045	1.94	0.24	Zocc08
18043142-2959515	4200	1.76	0.17	2.338[c]	3854	1.36	−0.49	Zocc08
18041770-3000304	4150	1.77	0.28	2.286[c]	4087	2.27	0.31	Zocc08
18045455-2958169	4550	1.95	−0.19	2.017[c]	4173	1.69	−0.22	Zocc08
18042994-3004324	4400	1.86	−0.11	2.074[c]	4144	2.00	−0.21	Zocc08
18045547-3003285	4300	1.98	0.43	2.435[c]	4039	1.78	0.14	Zocc08
18044764-3005147	4600	2.04	−0.65	2.234[c]	4149	1.66	−0.78	Zocc08
18043821-3003251	4350	1.99	0.34	2.452[c]	4163	2.46	0.35	Zocc08
18042236-3004162	4400	1.98	0.49	2.193[c]	4168	2.37	−0.02	Zocc08
18042178-3006128	4500	1.99	−0.25	1.959[c]	4124	1.57	−0.50	Zocc08
18043319-3009500	4500	1.94	0.02	2.155[c]	4210	1.96	−0.08	Zocc08
18042920-3006120	4150	1.76	0.38	2.256[c]	4151	2.41	0.37	Zocc08
18044899-3008077	4200	1.87	0.14	2.511[c]	4066	2.05	0.29	Zocc08
18041165-3009495	4400	1.91	0.46	2.193[c]	4049	1.87	0.30	Zocc08
18040840-3004382	4250	2.00	0.12	2.544[c]	3873	1.45	−0.036	Zocc08
18041566-3008540	4050	1.67	0.35	2.156[c]	4176	2.30	0.36	Zocc08
18044899-3008077	4200	1.87	0.14	2.511[c]	4066	2.05	0.29	Zocc08
18041165-3009495	4400	1.91	0.46	2.193[c]	4049	1.87	0.30	Zocc08
18040840-3004382	4250	2.00	0.12	2.544[c]	3873	1.45	−0.036	Zocc08
18041566-3008540	4050	1.67	0.35	2.156[c]	4176	2.30	0.36	Zocc08
18042205-3011214	4350	1.89	0.09	2.113[c]	4159	2.04	0.20	Zocc08
18041492-3007088	4400	2.01	−0.01	2.231[c]	3893	1.421	−0.20	Zocc08

Notes. Columns 2–4 list the stellar parameters as derived in the reference quoted in the last column. The APOGEE stellar parameters are listed in Cols. 5–7. [a] $(V - K)_0$ colour; [b] $(J - K)_0$ colour; [c] $(V - I)_0$ colour.

Table 1. continued.

2MASSid	$T_{\rm eff}$	$\log g$	[Fe/H]	Colour	$T_{\rm eff}^{\rm APOGEE}$	$\log g^{\rm APOGEE}$	[Fe/H]$^{\rm APOGEE}$	Ref.
18035975-3007473	4350	1.88	0.31	2.256^c	4046	1.84	0.24	Zocc08
18040535-3005529	4100	1.84	0.35	2.530^c	4049	2.27	0.50	Zocc08
18034164-3007549	4200	1.80	−0.12	2.407^c	3959	1.805	0.19	Zocc08
18040486-3003009	4500	2.00	−0.20	2.032^c	4105	1.87	−0.61	Zocc08
18040030-3004017	4300	1.85	0.08	2.157^c	3964	1.89	-0.73	Zocc08
18031997-3004274	4300	1.98	−0.17	2.398^c	3849	1.26	−0.30	Zocc08
18034052-3003281	4450	1.90	0.55	1.857^c	4486	2.24	−0.90	Zocc08
18031683-3006111	4650	2.02	−0.05	1.959^c	4181	1.95	−0.34	Zocc08
18033286-3005450	4200	1.94	0.28	2.384^c	4037	2.11	0.34	Zocc08
18040170-3001491	4600	1.99	−0.01	1.954^c	4118	2.65	−0.03	Zocc08
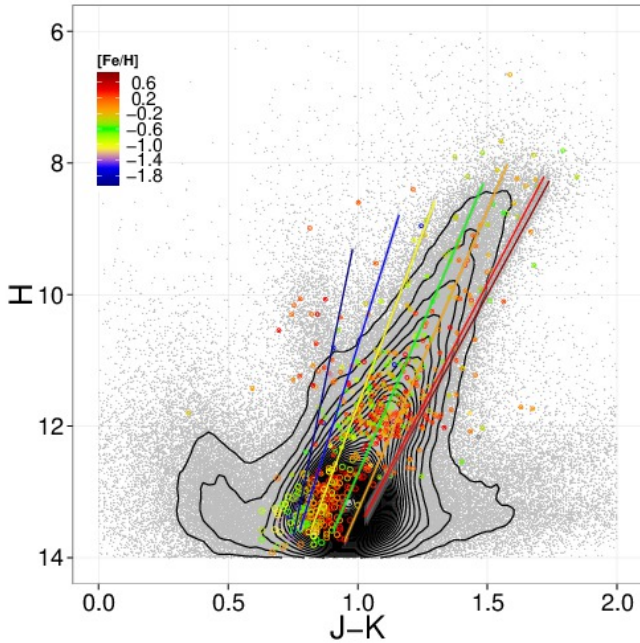
Fig. 2. 2MASS H vs. $J - K$ diagram for stars in BW. Superimposed over the individual star measurements are the density contours. The APOGEE targets are shown as filled circles; the GES targets are shown as open circles. The colour scale indicates the metallicity of the stars. Superimposed are the 10 Gyr PARSEC isochrones for different metallicities, colour-coded as in the legend.

Fig. 3. Distribution of the Galactocentric distances of our APOGEE sample. Grey bars indicate bulge stars (according to the left vertical scale), while the blue and red open histograms show the thick and the thin disc (according to the right vertical scale), respectively. The vertical dashed line defines our cut at $R_{\rm GC} = 3.5$ kpc to select likely bulge stars, while the vertical dotted line represents our cut at $R_{\rm GC} = 7.7$ kpc used to select the comparison disc sample (see Sect. 6).

3. Distances

The spectrophotometric distances and reddenings for the full sample were calculated using the stellar parameters $T_{\rm eff}$, $\log g$, and [Fe/H], together with 2MASS J, H, and $K_{\rm S}$ photometry and associated errors, to simultaneously compute the most likely line-of-sight distance and reddening by isochrone fitting with a set of PARSEC isochrones. We used the same method as presented in Rojas-Arriagada et al. (2017), considering a set of isochrones in the age range from 1 to 13 Gyr in 1 Gyr steps and metallicities from −2.2 to +0.5 in steps of 0.1 dex. We chose this method to calculate the distances consistently with respect to the bulge sample of the GES. A comparison was made with the distance code of the "BPG group" (Santiago et al. 2016), which uses a Bayesian approach. We did not find any systematic offset in the distance distribution.

Figure 3 displays the histogram of our BW sample as grey bars. The peak of the histogram is located close to the distance of the Galactic Centre ($R_{\rm GC} = 0$ kpc), and then decreases towards

larger distances. For the discussion of the MDF (Sect. 5) we restrict our sample to $R_{\rm GC} < 3.5$ kpc to ensure a sample of stars likely located in the Galactic bulge. This selection criterion leaves us with 269 stars. The two open histograms in Fig. 3 show the distribution of APOGEE disc stars, from which we selected a comparison subsample. The definition of this disc sample is discussed in Sect. 6.

4. Comparison of stellar parameters

Figure 4 presents the comparison of the effective temperatures between Rich05, Ful06, Zocc08, and Ryde10. Table 2 gives the corresponding mean differences and the standard deviation of the stellar parameters with respect to APOGEE. The Rich05 and the Zocc08 stars exhibit systematically higher temperatures (177 K and 255 K, respectively) compared to APOGEE, while Ful06 and Ryde10 obtain similar temperatures (15 K and 61 K). The largest dispersion appears for the Ful06 stars and for the Zocc08 stars (186 K and 161 K, see Table 2), while
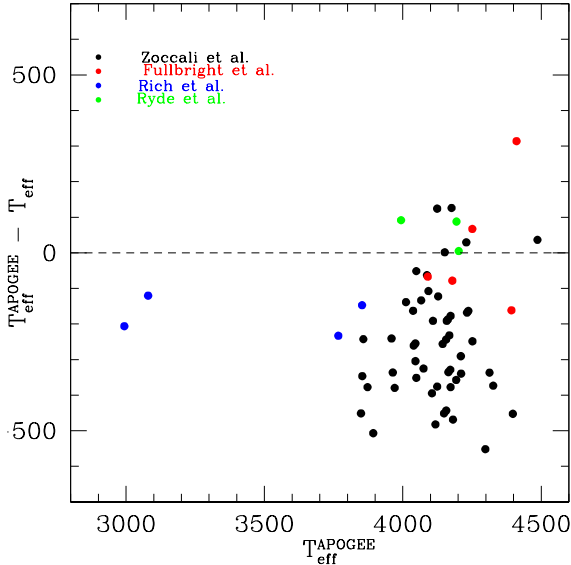
Fig. 4. Difference in $T_{\rm eff}$ between APOGEE and literature values vs. $T_{\rm eff}$. Black circles are giants from Zoccali et al. (2008), red circles are from Fulbright et al. (2006), blue circles are from Rich & Origlia (2005), and green circles are from Ryde et al. (2010).

Table 2. Difference between stellar parameters from APOGEE compared to the literature (Δ) and its rms dispersions of the differences (σ) for stellar parameters $T_{\rm eff}$, $\log g$, [Fe/H], and α.

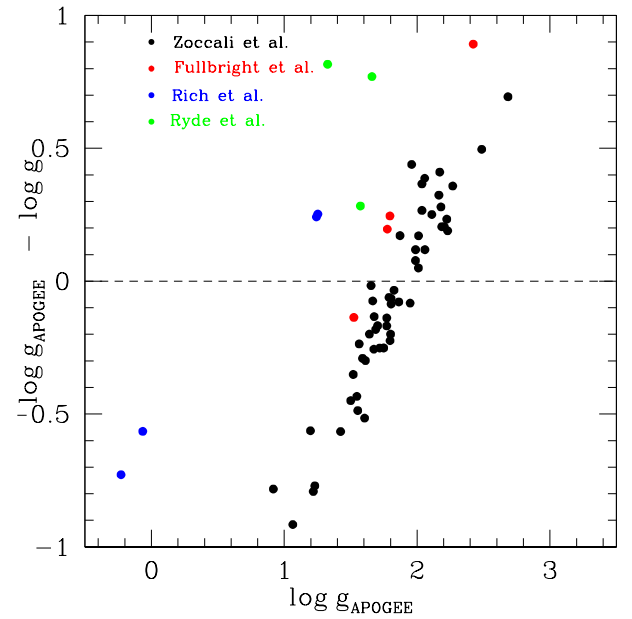|	Rich05	Ful06	Zocc08	Ryde10	
$\langle \Delta T_{\rm eff} \rangle$	–177	15	–255	61	[K]
$\sigma(T_{\rm eff})$	52	186	161	49	[K]
$\langle \Delta \log g \rangle$	–0.19	0.48	–0.12	0.62	[dex]
$\sigma(\log g)$	0.52	0.54	0.48	0.29	[dex]
$\langle \Delta[{\rm Fe/H}] \rangle$	–0.18	0.13	0.10	0.18	[dex]
$\sigma([{\rm Fe/H}])$	0.14	0.09	0.28	0.09	[dex]
$\langle \Delta[\alpha/{\rm Fe}] \rangle$	–0.19	–0.19	–0.07	–0.13	[dex]
$\sigma([\alpha/{\rm Fe}])$	0.11	0.10	0.15	0.06	[dex]

Fig. 5. Difference in $\log g$ between APOGEE and literature values vs. $\log g$ using the same symbols as in Fig. 4. A clear linear relation is seen for the Zocc08 sample between the difference of the spectroscopic and photometric gravities with respect to the spectroscopic $\log g$ values (see text).

the dispersion in Ryde10 and Rich05 is rather small (49 K and 52 K). In our comparison sample (see Fig. 4), the effective temperatures of Ful06 were determined based on photometric $V - K$ colours, and on differential excitation temperatures and ionization temperatures. They found in general a very good agreement between these three temperature estimates with a small scatter. Zocc08 uses $V - I$ colours as a first estimate, while the final Zocc08 values, which we adopted here for comparison, were estimated spectroscopically by imposing excitation equilibrium on a set of ~60 FeI lines. Rich05 estimated temperatures based on $J - K$ colours, while Ryde10 uses the effective temperatures of Ful06.

One part of the wide range of photometric temperatures compared to the spectroscopic values of APOGEE can be explained by the inhomogeneous use of photometric colours in the comparison work, while the spectroscopic temperatures from APOGEE were determined in a homogeneous way. We indicate in Table 1 the corresponding photometric colours as well as the photometric system used. González Hernández & Bonifacio (2009) studied in detail the effective temperature scale using the infrared flux method. They show in their Table 5 that the $V - K$ colours show the smallest dispersion in the determination of the effective temperature (~30 K) and should therefore be used for photometric temperatures. The $V - I$ colours and especially the $J - K$ colours show, on the other hand, a much larger dispersion in the effective temperature. Clearly, much more effort is needed to understand the difference between spectroscopic and photometric temperature determinations.

Figure 5 shows the APOGEE-literature comparison of surface gravity. The surface gravities of APOGEE are calibrated with respect to the asteroseismic $\log g$ estimates from NASA's *Kepler* mission (Borucki et al. 2010). The applied offset is about 0.2 dex for stars with solar metallicities. The typical dispersion between photometric $\log g$ and spectroscopic estimates are of the order of ±0.5 dex, while the dispersion in Ryde10 is slightly lower (0.3 dex) although they exhibit a large offset (0.62 dex). In general, there is a large systematic discrepancy between photometrically derived $\log g$ and spectroscopic estimates.

The Zocc08 photometric $\log g$ estimates display a clear linear behaviour with respect to APOGEE. In Zocc08, the photometric gravities were estimated by assuming a mean stellar mass of $M = 0.8\ M_\odot$ and a sample distance of 8 kpc. The dispersion of their $\log g$ is about 0.25 dex and is due to the intrinsic depth of the Galactic bulge (Lecureur et al. 2007). We investigate the effects of these assumptions by selecting stars from a TRILEGAL (Girardi et al. 2012) simulation using the Zocc08 photometric selection function (see their Fig. 1), and calculating photometric $\log g$ values. Figure 6 displays the selected simulated stars in the same plane as in Fig. 5, colour-coded by the difference of their true distances with respect to an assumed mean field distance ($\overline{d_{\rm BW}}$). Given the relatively narrow magnitude selection of Zocc08, stars at greater distances than $\overline{d_{\rm BW}}$ are intrinsically luminous (low $\log g$ values), but appear fainter. By assuming these stars are at $\overline{d_{\rm BW}}$, the resulting photometric $\log g$ values are higher, to account for their apparent low luminosity, determining a $\Delta \log g$(true – phot) < 0. Conversely, foreground stars at distances shorter than $\overline{d_{\rm BW}}$, are on average intrinsically less luminous (high $\log g$ values). By assuming these stars are at $\overline{d_{\rm BW}}$, the resulting photometric $\log g$ values are smaller,
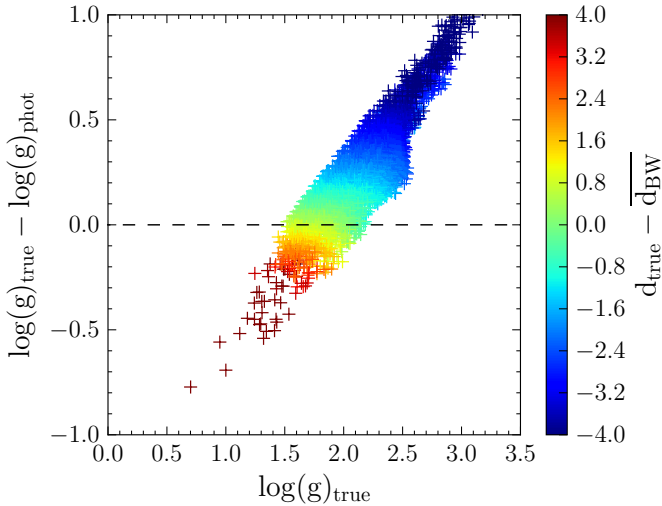
Fig. 6. Difference in log g for stars selected from a TRILEGAL simulation of BW as a function of log g (true). The photometric values were computed by assuming the whole sample is at a distance of 8 kpc. Symbols are colour-coded according to the difference of the true distance with respect to that assumption. Photometric gravities become smaller with respect to the true spectroscopic surface gravities if the assumed distance is shorter than 8 kpc.

to account for their apparent high luminosity, determining a $\Delta \log g(\mathrm{phot}-\mathrm{spec}) > 0$. The interplay between these complementary effects determines the linear trend observed in Fig. 5 and reproduced in Fig. 6. The dispersion around the mean occurs because for a given distance interval there are stars spanning a range of true log g values. If we consider that the reddening in BW is small and homogeneous, photometric log g estimates in other windows of the Galactic bulge, where interstellar extinction is higher and spatially patchy, could lead to even larger uncertainties.

Figure 7 shows the comparison of the global metallicities. Except for Rich05, the comparison samples predict metallicities that are generally too low with respect to APOGEE. The offset can go up to 0.18 dex (Ryde10). The typical dispersion is about 0.15 dex, but is significantly larger for the Zocc08 sample (0.28 dex), where stars with [M/H] < 0 are systematically more metal-poor with respect to the APOGEE measurements. This larger scatter is partially due to the larger dispersion in T_{eff} and log g (see Figs. 4 and 5) of the Zocc08 determinations.

For the comparison of the α-elements, we used the combination of Mg and Si for Rich05 and Ful06, the Gonzalez et al. (2011a) values for the Zocc08 sample, and the global α-element estimate for Ryde10. In general, the α-element abundances in APOGEE are lower than the literature values with differences ranging from 0.07 dex (Zocc08) up to 0.19 dex (Rich05, Ful06). The dispersion is about 0.1 dex, where again Zocc08 has a larger dispersion (0.15 dex).

5. Metallicity distribution function

The MDF of BW stars is an important tool that can be used to unravel the mix of stellar populations that comprise the Galactic bulge. With larger sample sizes, it becomes clear that the MDF does not reflect a single stellar population, but reveals at least a bimodal nature. This behaviour was previously noticed by Hill et al. (2011), and was further characterized by Babusiaux et al. (2010), who found metal-rich stars displaying bar-like kinematics in contrast with the isotropically hotter metal-poor bulge.
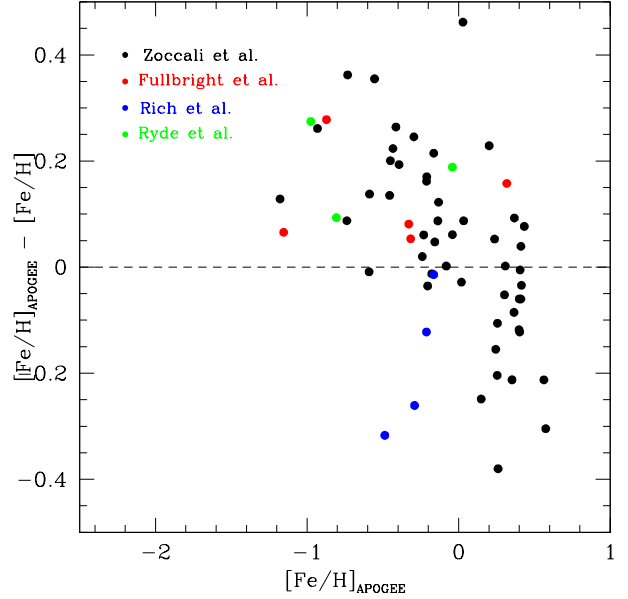
Fig. 7. Difference in [Fe/H] between APOGEE and literature values vs. [Fe/H] using the same symbols as in Fig. 4. The typical dispersion is about 0.1 dex, while the dispersion increases significantly for the Zocc08 sample (~0.28 dex).
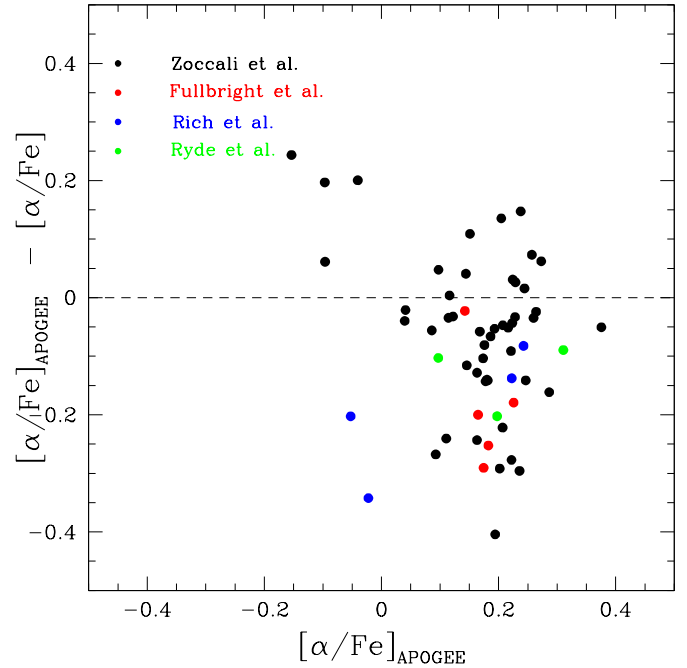

Fig. 8. Difference in [α/Fe] between APOGEE and literature values vs. [α/Fe]. The symbols are the same as in Fig. 4. The typical dispersion is 0.1 dex, with a slightly higher value for the Zocc08 sample (~0.15 dex).

Figure 9 compares the BW MDF as sampled by APOGEE with two other recent large-scale spectroscopic surveys, the ARGOS (in m0m5, a field close to BW; Freeman et al. 2013; Ness et al. 2013) and the GES (iDR1 Gilmore et al. 2012; Rojas-Arriagada et al. 2014; Mikolaitis et al. 2014). In each case, we used spectrophotometric distances to select samples of likely bulge stars as those with Galactocentric distance satisfying $R_{\mathrm{GC}} < 3.5$ kpc, as was done for the APOGEE sample (Sect. 3). The visual inspection of the metallicity distributions of these likely bulge stars, as depicted by the histograms in each panel, reveals some qualitative differences. While the GES and
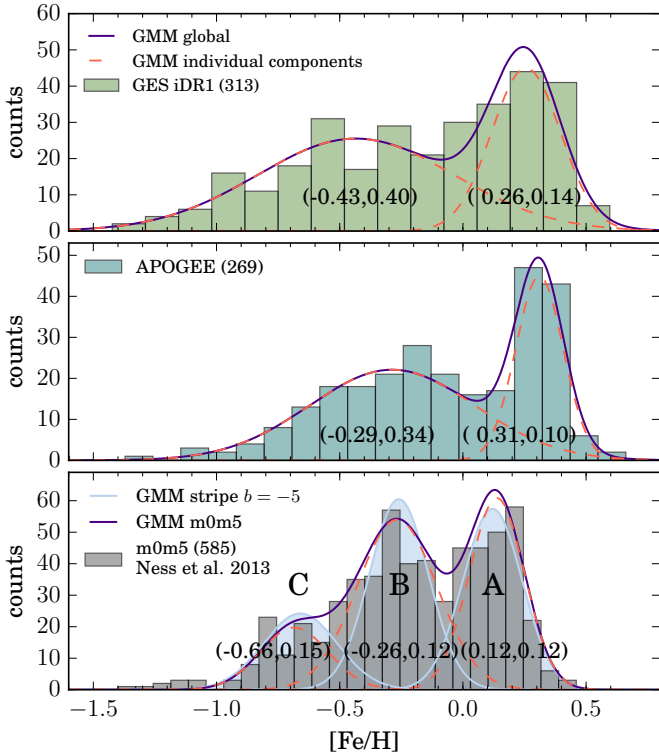
Fig. 9. Metallicity distribution function for stars in BW. Only sources with $R_{GC} < 3.5$ kpc are included. *Top panel*: MDF of the GES BW data (iDR1). *Middle panel*: MDF of the APOGEE data. In each case, the GMM decomposition is depicted by dashed (individual components) and solid (global profile) lines, with mean and width values in parentheses. *Lower panel*: MDF of the closest field to BW from ARGOS data (Ness et al. 2013). The GMM decomposition is depicted as in the other panels. For comparison, the GMM decomposition of the $b = -5°$ strip, as taken from Ness et al. (2013), is depicted by the three Gaussian profiles, with the corresponding mean and width values quoted in parentheses.

APOGEE samples can be described with bimodal distributions, the ARGOS sample apparently requires a third component.

To quantify the substructure of the different MDFs, we perform a Gaussian mixture model (GMM) decomposition independently for each case. A GMM is a parametric probability density function given by a weighted sum of a number of Gaussian components. The GMM parameters are estimated as those that provide the best representation of the data set density distribution structure. The expectation-maximization algorithm determines the best parameters of a mixture model for a given number of components. Since, in the general case, the number of components is not known beforehand, an extra loop of optimization is required to compare several optimal models with different numbers of components. To perform this task, we adopted the Akaike information criterion (AIC) as a cost function to asses the relative fitting quality between different proposed mixtures. In the case of the GES and APOGEE samples, the AIC gave preference for a two-component solution with centroid and width values as quoted in each panel. The narrow metal-rich component is quite similar in both data sets, while the metal-poor one is broader and relatively more metal-poor in the GES data.

The ARGOS MDF was found in Ness et al. (2013) to be composed of up to five metallicity components, with the three most metal-rich (designated as A, B, and C: [Fe/H] > −1.0 dex) accounting for the majority of stars. In that work, three general MDFs were assembled from samples in fields located in

three latitude stripes (±15° in longitude) at $b = -5°, -7.5°,$ and −10°. Their GMM analysis yielded a three-component solution in each case. In particular, in the lower panel of Fig. 9, we display in light blue the three Gaussian components resulting from their analysis of the $b = -5°$ stripe. For verification, we performed a GMM analysis on the m0m5 field sample, which is depicted by the histogram. The best model is a mixture of three Gaussians with means of $\mu = -0.69, -0.27, 0.14$ and dispersions of $\sigma = 0.14$ dex, 0.16 dex, 0.11 dex, in good agreement with the Ness et al. (2013) results for the entire $b = -5°$ strip, as quoted in the lower panel of Fig. 9.

The trimodal metallicity distribution of the ARGOS data is visible in the individual field distributions and in the merged strip samples. This feature might be an imprint of the parametrization performed on the ARGOS data, but it could also arise as an effect of assembling samples over a large longitudinal area where small systematic variations in the intrinsic shape of the bulge MDF are possible. In particular, the trimodal nature of the ARGOS parametrization could come from the fact that ARGOS uses effective temperature estimates from $(J − K)_0$ colours (Freeman et al. 2013), which can result in systematic differences (see Fig. 4) compared to spectroscopically derived temperatures. Recio-Blanco et al. (2016) estimated the end-of-mission expected parametrization performances of the *Gaia* DPAC pipeline (GSP-Spec) used for the derivation of the atmospheric parameters and chemical abundances from the RVS stellar spectra ($R = 11\,200$). The spectral resolution, as well as the spectral region, of the *Gaia*-RVS is very similar to that of ARGOS. Recio-Blanco et al. (2016) showed, based on model spectra (see their Fig. 21), that an error of 100 K can easily result in at least 0.1 dex errors in [Fe/H] with a significantly large dispersion that gets larger for cooler stars. An effect such as this could be the reason for the additional third component in the observed MDF of ARGOS. On the other hand, the bimodality of the bulge MDF has been characterized by a number of studies examining specific locations in the bulge region (Uttenthaler et al. 2012; Gonzalez et al. 2015), and by the results of the fourth internal data release of the GES (Rojas-Arriagada et al. 2017), which covers a larger area. To understand the difference between the ARGOS data set and those of APOGEE and GES, a common set of observed stars covering the full metallicity range – which is currently not available – is necessary. In the end, this discrepancy highlights that understanding the number of metallicity-distinguished components constituting the bulge is an important and unresolved issue warranting further investigation.

6. Trends in the abundance-metallicity plane

The distribution of stars from a given population in the abundance-metallicity plane encodes important information about its star-formation history and chemical evolution. In particular, detailed comparisons between the bulge and other Galactic components in the [α/Fe] vs. [Fe/H] plane can provide a direct means of unraveling the origin of the bulge in the context of other Galactic stellar populations.

Figure 10 displays our BW APOGEE sample in the [Mg/Fe] vs. [Fe/H] plane. To compare this data with the GES, we overplot the median trend of its BW stars, as determined by dividing the sample into narrow metallicity bins (Rojas-Arriagada et al. 2017). To assess the statistical significance of the resulting profile, a shaded area depicts the standard error of the mean. To enhance the comparison, we computed in the same manner the median trend of the bulge APOGEE sample studied
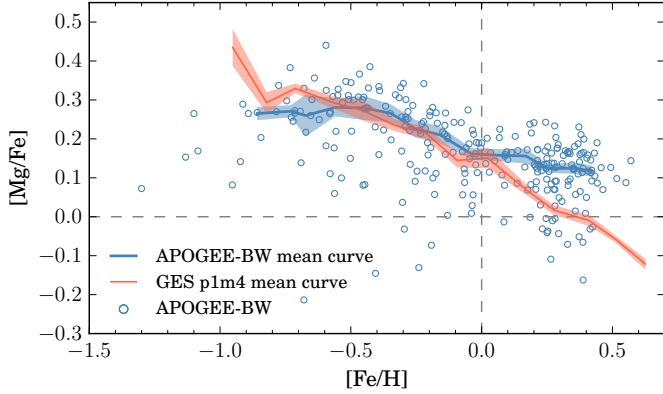
Fig. 10. Baade's window stars in the [Mg/Fe] vs. [Fe/H] plane. The APOGEE sample and its median trend (blue open circles and blue line, respectively) are compared with the mean trend of BW stars from the fourth internal data release of the GES (red line). A shaded red area around the mean trend depicts the standard error of the mean.

Fig. 11. [Mg/Fe] vs. [Fe/H] for thin disc (brown points), thick disc (blue points), and BW (red crosses) stars. Median trends are computed for the discs (dashed lines) and the bulge (solid line) in small metallicity bins as a visual aid. Bulge stars appear to be on average more α-enhanced than the thick disc.

here. The abundance scale of APOGEE agrees remarkably well with that of the GES. The GES stars are on average slightly less α-enhanced than APOGEE stars, by about 0.02 dex over the common metallicity range. There is a clear discrepancy between the α-element abundances between APOGEE and GES for the more metal-rich stars ([Fe/H] > -0.1), in the sense that the GES obtains lower α-element abundances. The difference is $\sim$0.1 dex at [Fe/H] = $+0.2$ and increases to $\sim$0.15 dex at [Fe/H] = $+0.4$ dex. APOGEE derives Mg abundances from four different spectral windows (centred at 1.533, 1.595, 1.672, 1.676 μm), all of them in the infrared H band (see García Pérez et al. 2016), while GES uses the lines at 8717.8 Å, 8736.0 Å, and 8806.7 Å in the optical spectral range. A part of the differences between APOGEE and GES could arise from differences in atomic data, although one has to be aware that abundance determination for metal-rich giants, like those used in these two studies, is challenging and systematic effects from other sources would not be surprising.

This comparison emphasizes the necessity of a common sample of stars well-distributed in the $T_{\rm eff}$-log(g)-[Fe/H] space to cross-calibrate abundance measures coming from different surveys.

In Fig. 11 we attempt a direct homogeneous comparison between the distributions of disc and bulge stars in the abundance-metallicity plane, using results exclusively from APOGEE. To this end, we selected a sample of disc stars (namely, stars in pointings with $|l| \geq 15^{\rm o}$ and $|b| \geq 15^{\rm o}$), cleaning it based on several flags provided by the ASPCAP pipeline. In addition, we selected stars with $R_{\rm GC} < 7.7$ kpc (dotted line in Fig. 3) to have a sample representing the chemical distributions inside the solar circle, without decreasing the sample size significantly. To minimize the systematics arising from the comparison of stars with different fundamental parameters, we selected disc stars in the same range of $T_{\rm eff}$ and log g spanned by our BW sample. Application of all of the previous cuts yield a final sample of 2904 stars.

The selected disc stars present a distribution in the abundance-metallicity plane with a clear gap separating a high-α and low-α sequences (see also Hayden et al. 2015). We divide the sample by performing a clustering analysis in narrow metallicity bins. The resulting thin- and thick-disc samples (brown and blue points, respectively), together with the BW bulge sample (red crosses), are depicted in Fig. 11. To aid visualization of their
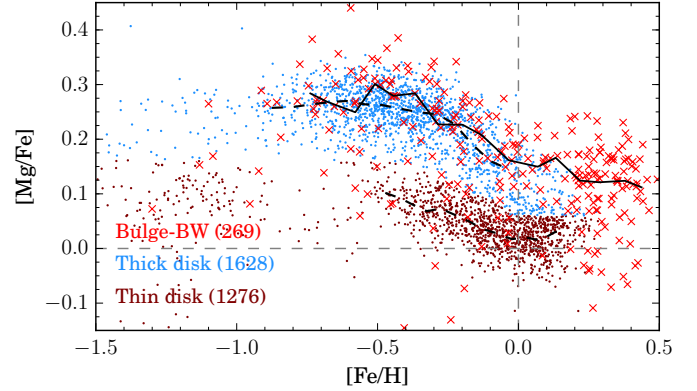
distributions, we compute a median trend for the discs (dashed lines) and the bulge (solid line). Interestingly, bulge stars appear to be on average more α-enhanced than the thick disc, reaching higher metallicity values. This may be the result of a difference in the relative formation timescales, where that of the bulge is faster and dominated by massive stars. The confirmation of this feature is of clear importance in our quest for disentangling the different natures and origins of the stellar populations that co-exist in the central kiloparsecs of the Galaxy.

There are a small number of stars with low magnesium abundances. Their relative proportion does not decrease significantly if we apply a more stringent cut in Galactocentric distances, which means that if we account for the large errors in spectrophotometric distances these stars appear to be located inside the bulge region. Recio-Blanco et al. (2017) found from GES Bulge data a small fraction of low-α stars that have chemical patterns compatible with those of the thin disc, indicating a complex formation process of the Galactic bulge.

7. Age distribution

Obtaining accurate ages for stars in the Galactic bulge is a crucial ingredient in the comparison of observed data to chemo-dynamical evolutionary models. Recently, Martig et al. (2016) developed a new method for estimating masses and implied ages for giant stars based on C and N abundances calibrated on astero-seismic data. They demonstrate that the [C/N] ratio of giants decreases with increasing stellar mass, as expected from stellar-evolution models. We use the relation of Martig et al. (2016) from Appendix A.3, and adopt the same cuts as those authors to ensure the reliability of the relation: $4000 < T_{\rm eff} < 5000$ K, $1.8 <$ log $g < 3.3$, [M/H] > -0.8, $-0.25 <$ [C/M] < 0.15, $-0.1 <$ [N/M] < 0.45, $-0.1 <$ [(C + N)/M] < 0.15, and $-0.6 <$ [C/N] < 0.2. This leaves only 74 stars; Fig. 12 shows the age distribution of stars with metallicity lower and higher than [Fe/H] = -0.1 dex [3] (to roughly separate stars into the two modes of the MDF; see Fig. 9). Given the small size of the sample, we use generalized histograms (kernel of 1.5 Gyr) to avoid the effect of binning of conventional histograms, and a bootstrap analysis to asses for the significance of the resulting distributions. To this end, we performed 600 bootstrap resamplings

---

[3] The results below do not qualitatively change if the cut is done at ± 0.1 dex from this limit.

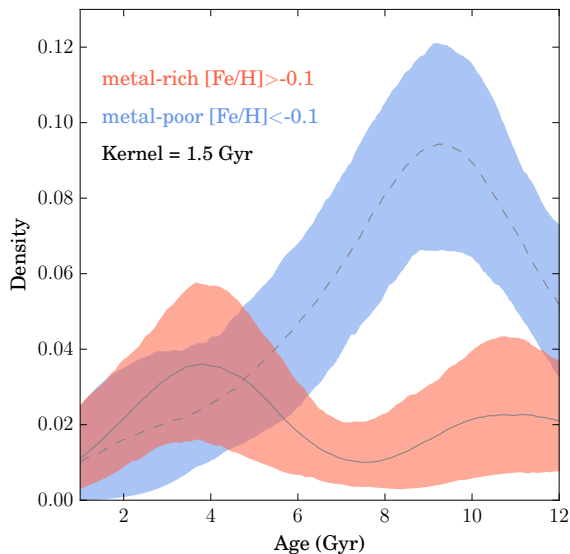**Fig. 12.** Age distribution of stars in BW using the formula of Martig et al. (2016). Only sources with $4000 < T_{\text{eff}} < 5000$ K, $1.8 < \log g < 3.3$, [M/H] > -0.8, $-0.25 < $ [C/M] < 0.15, $-0.1 < $ [N/M] < 0.45, $-0.1 < $ [(C + N)/M] < 0.15, and $-0.6 < $ [C/N] < 0.2 were taken into account. From a bootstrap analysis on generalized histograms (kernel 1.5 Gyr), mean trends (solid and dashed grey lines), and error bands to the $\pm 2\sigma$ level (shaded coloured areas) are derived for metal-rich and metal-poor stars (cut at [Fe/H] $= -0.1$ dex) as percentiles of the 600 bootstrap resamplings.

of the metal-rich and metal-poor samples, computing median trends (solid and dashed grey lines) and error bands (shaded areas) at the $\pm 2\sigma$ level from percentiles.

The peak of the distribution of metal-poor stars is about ~10 Gyr, with a decreasing tail toward younger ages. This compares well with the mean bulge age as estimated from photometric data (Zoccali et al. 2003; Clarkson et al. 2008, Valenti et al. 2013). On the other hand, the generalized distribution of metal-rich stars shows a flatter distribution, with two overdensities of young and old stars. This seemingly bimodal age distribution for metal-rich stars is comparable with the results of Bensby et al. (2013), who found from their sample of dwarf and subgiant microlensed stars that while metal-poor bulge stars are uniformly old, metal-rich bulge stars span a broad range of ages ($2-12$ Gyr), with a peak at $4-5$ Gyr. Recently, Haywood et al. (2016) concluded, from deep HST data in the SWEEPS field, that a certain fraction of young stars is necessary to reproduce the observed colour-magnitude diagram (CMD). In their model, about 50% of the stars have ages greater than 8 Gyr, suggesting that there might be a fraction of young stars in their CMD. If we extrapolate their results to BWs, according to their model we would expect 35% of the stars to be younger than 8 Gyr. We find a very similar fraction to that seen in Fig. 12. However, their model reports that metal-rich stars with [Fe/H] > 0.0 are all younger than 8 Gyr, while our small sample suggests that metal-rich stars can be either young or old. We also note that the younger population exhibit, on average, less α-element enhancement than the old population (alpha$_{\text{mean}}$ = 0.126 for ages < 6 Gyr and alpha = 0.215 for ages > 6 Gyr). Overall, our age distributions derived from chemistry seem robust, despite the sample size, and constitute an independent verification of results suggested from isochrone fitting to fundamental parameters (Bensby et al. 2013) and photometric data (Haywood et al. 2016). However, we want to stress that the ages derived from [C/N] abundances have to be considered

with caution. As discussed by Martig et al. (2016), the absolute scaling of the derived ages might be slightly off. This leads, for example, to underestimated ages of old stars, as shown in their Fig. 11. In addition, owing to our small sample of stars, more data are clearly necessary to better constrain the bulge age distribution and its metallicity dependence.

8. Individual chemical abundances

Compared to the 15 individual elemental abundances determined in DR12 (Holtzman et al. 2015), the DR13 results include seven new elements: P, Cr, Co, Cu, Ge, Rb, and Nd; in total, DR13 includes elemental abundances for the 22 elements C, N, O, Na, Mg, Al, Si, P, S, K, Ca, Ti, V, Cr, Mn, Co, Ni, Cu, Ge, Rb, Y, and Nd. However, we only discuss the abundances for 11 of these elements in this section. The reasons for the exclusion of the other 11 elements are as follows:

– We do not include C and N abundances because a giant star which ascends the giant branch deepens the convective envelope and the star experiences the first dredge-up. This means that CNO-processed material containing a lot of N but depleted in C is brought to the surface. This is nicely shown in Fig. 1 of Martig et al. (2016). It also turns out that the depth of the convective envelope and the amount of CNO-cycling in the core depends on the mass of the star, a fact that we use to get ages for the stars in our Sect. 7. This means that giants cannot be used to trace the galactic chemical evolution of C and N: the abundances simply do not reflect the abundances of their birth. This is shown in the lower panel of Fig. 2 in Martig et al. (2016).

– The spectral lines used to determine the P abundances are generally very weak in the type of giants observed in BW. Holtzman et al. (in prep.) caution that these lines are weak and uncertain, while Hawkins et al. (2016) derive only upper limits in their independent analysis of APOGEE spectra. We therefore exclude this element in the discussion below.

– The abundance-trend of S for the BW stars is very scattered as compared to our sample of local disc stars, possibly because the S abundance is in principle derived from a single, blended line, and higher S/N than the already high S/N of the BW spectra are needed to trace this element with certainty. We therefore exclude this element in the discussion below.

– The DR13 abundance trends of Ti in the local discs do not resemble the expected α-element trends found in many other works. The reason for this behaviour is described in Hawkins et al. (2016), as possible 3D/NLTE-effects in the Ti I lines used in DR13. We therefore exclude this element in the discussion below.

– The abundance trend of V in the BW stars is very scattered. The V abundances are mainly determined from two lines, of which one is quite weak but the other is of suitable strength. It is possible that the V abundance trend in the bulge would be less scattered if the weak line were to be excluded in the analysis. We also note that Hawkins et al. (2016) derive a different V trend for their independent analysis of a subsample of APOGEE-spectra. For these reasons, we exclude this element in the discussion below.

– The Cu, Ge, Rb, Y, and Nd abundances are all determined from few, often single, weak and blended lines. We therefore exclude these elements in the discussion below.

To conclude, we discuss the abundances of the following 11 elements in this section: O, Na, Mg, Al, Si, K, Ca, Cr, Mn, Co, and Ni.
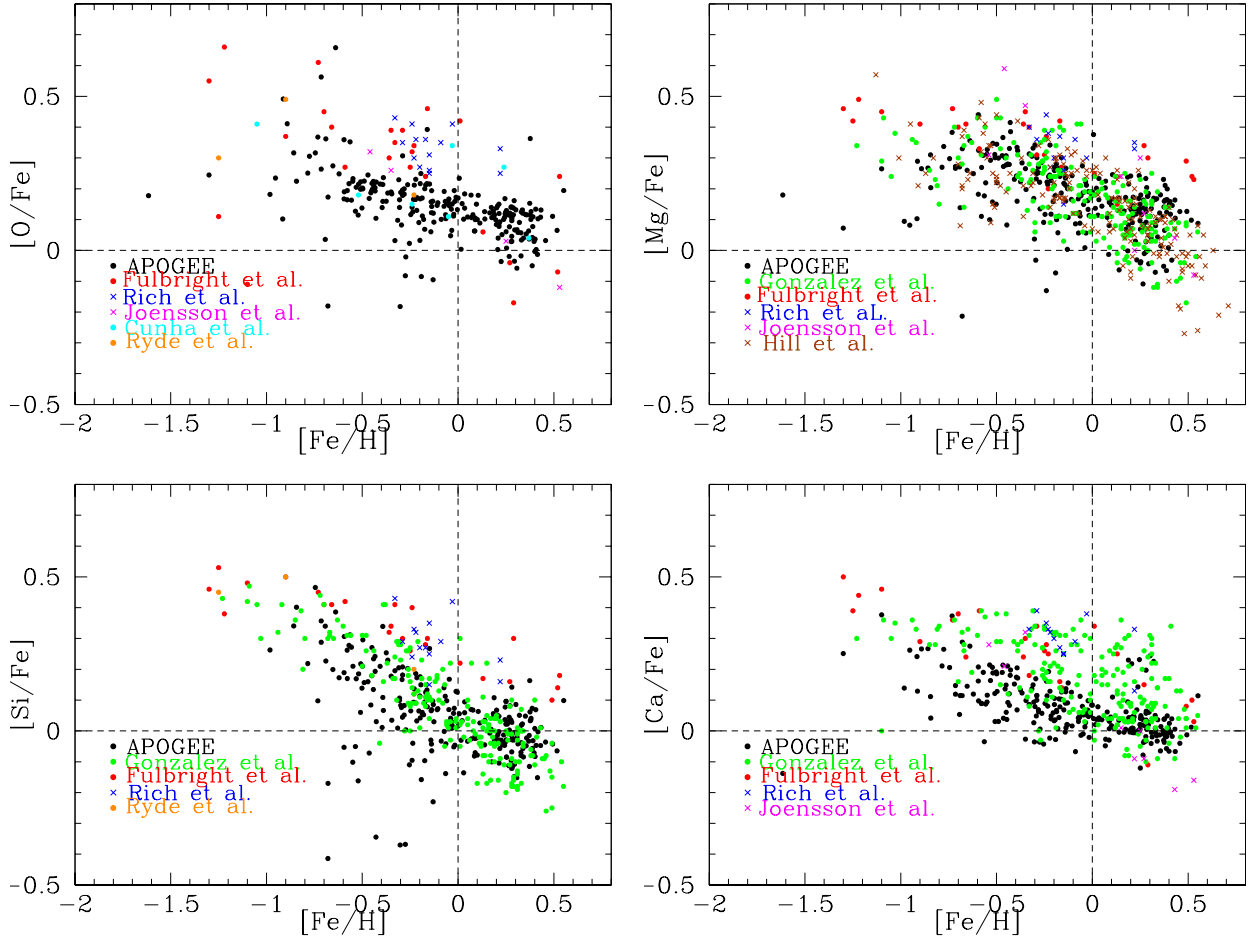
Fig. 13. [Fe/H] vs. [X/Fe] of APOGEE stars in BW for α-elements compared with literature values.

8.1. The α-elements: O, Mg, Si, and Ca

Figure 13 shows the trends of the α-elements (O, Mg, Si, Ca) compared to available literature values for M giants. These abundances are of particular interest because accurate [α/Fe] ratios place strong constraints on the star-formation history (e.g. Matteucci & Brocato 1990) in a stellar population. In addition to the previously mentioned references, we add that of Jönsson et al. (2017), who determined elemental abundances of O, Mg, and Ca of bulge K giants using the high-resolution ($R \sim 47\,000$) UVES/FLAMES spectrograph at the VLT.

Oxygen abundances determined in Rich05, Cunha06, Fulbright et al. (2007b), Ryde10, and Jönsson et al. (2017) are presented in the top left panel of Fig. 13. The APOGEE O abundances are lower than those of Rich05 and Fulbright et al. (2007b), while they are comparable to those of Cunha06, Ryde10, and Jönsson et al. (2017).

Magnesium abundances are determined in Rich05, Fulbright et al. (2007b), Gonzalez et al. (2011a), Hill et al. (2011), and Jönsson et al. (2017); these abundances are displayed in the top right panel of Fig. 13. The APOGEE Mg abundances exhibit generally good agreement with the trends found by Gonzalez et al. (2011a) and Hill et al. (2011). The Rich05, Fulbright et al. (2007b), and possibly Jönsson et al. (2017) stars are slightly enhanced in Mg compared to APOGEE, in particular in the metal-rich regime ([Fe/H] > 0.2).

Silicon abundances are determined in Rich05, Fulbright et al. (2007b), Ryde10, and Gonzalez et al. (2011a), and all abundances are shown in the bottom left panel of Fig. 13. The

APOGEE Si abundances are in general agreement with Ryde10 and Gonzalez et al. (2011a), while Rich05 and Fulbright et al. (2007b) derive systematically higher Si abundances.

Calcium abundances are determined in Rich05, Fulbright et al. (2007b), Gonzalez et al. (2011a), and Jönsson et al. (2017). Those abundances are plotted in the bottom right panel of Fig. 13. The APOGEE Ca abundances are systematically about 0.15 dex lower than the values reported in Rich05, Fulbright et al. (2007b), and Gonzalez et al. (2011a). Jönsson et al. (2017) report similar low Ca abundances to those APOGEE. The dispersion in APOGEE is much smaller than that reported in e.g. Gonzalez et al. (2011a), for a given metallicity, resulting in a narrow Ca sequence for the metallicity range $-1 < [Fe/H] < 0.5$.

8.2. The iron-peak elements: Cr, Mn, Co, and Ni

Unlike the lighter elements, the abundance patterns of Fe-peak elements in the Galactic bulge have not been well explored, and only a few studies exist for comparison. Johnson et al. (2014) investigated chemical abundances of α-elements and heavy Fe-peak elements such as Cr, Co, and Ni, for RGB stars roughly 1 mag above the clump in the Galactic bulge, although not in BW. Owing to the lack of comparison samples for the iron-peak elements, we have chosen to include this reference. McWilliam et al. (2003) studied manganese in BW, and found that the bulge [Mn/Fe] trend is approximately the same as that found in the solar neighbourhood disc, and also for halo stars, and even follows the local [Mn/Fe] trend for metal-rich
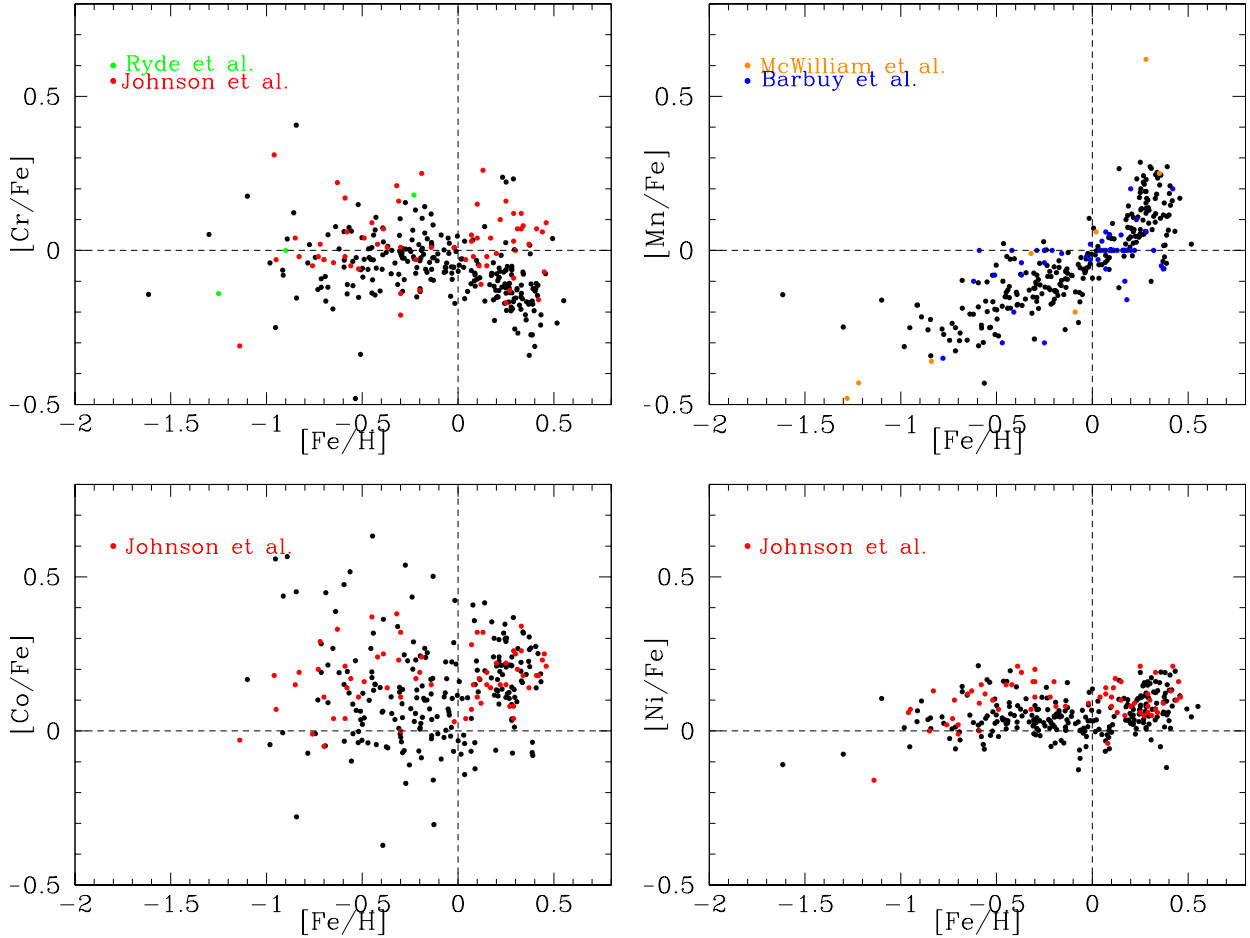
Fig. 14. [Fe/H] vs. [X/Fe] of APOGEE stars in BW for iron-peak elements compared with literature values.

stars. Barbuy et al. (2013) obtained Mn measurements of 56 red giants using the high-resolution FLAMES/UVES spectra for four Galactic bulge fields, and concluded that the behaviour of [Mn/Fe] vs. [Fe/H] shows that the iron-peak element Mn has not been produced in the same conditions as other iron-peak elements such as Fe and Ni.

The production sites for these elements are uncertain, and the stellar yields of these elements remain under debate (Battistini & Bensby 2015). The elements Mn and Co are believed to be produced mainly by explosive silicon burning in SNII (Woosley & Weaver 1995), while to a smaller extent in SNIa (Bravo & Martínez-Pinedo 2012).

Manganese exhibits an increasing trend with increasing metallicity (top right panel of Fig. 14), both for our determinations and for the literature values. There is a well-defined [Mn/Fe] trend in the metallicity range −0.7 < [Fe/H] < +0.2; while for the most metal-rich stars ([Fe/H] > 0.2) the Mn abundances have a larger scatter at a given [Fe/H]. Battistini & Bensby (2015) have shown that the Mn trends can change drastically if NLTE corrections are used, resulting in [Mn/Fe] becoming basically flat with metallicity. The increasing [Mn/Fe] trend is consistent with previous studies for the thick disc and halo stars in the range −1.5 < [Fe/H] < 0.0 (Prochaska et al. 2000; Nissen et al. 2000). For [Fe/H] > −1, the increasing [Mn/Fe] with increasing [Fe/H] is interpreted as an onset of contribution from Type Ia SNe (Kobayashi et al. 2006).

The behaviour of [Co/Fe] vs. [Fe/H] is shown in the bottom left panel of Fig. 14. The [Co/Fe] ratio exhibits low-level

variations as a function of [Fe/H] but is generally enhanced with [Co/Fe] = +0.15, which is similar to that observed by Johnson et al. (2014).

Johnson et al. (2014) reported that [Cr/Fe] = 0.0 for the full metallicity range, and that the abundance patterns of [Cr/Fe] are very similar to the thin disc and thick disc stars. The top left panel of Fig. 14 reveals similar [Cr/Fe] trends for [Fe/H] ≤ 0.0, but contrary to Johnson et al. (2014), our [Cr/Fe] trend decreases for [Fe/H] > 0.

The [Ni/Fe] ratio displays similar variations to [Co/Fe], but at a much smaller amplitude, and is slightly enhanced with [Ni/Fe] = +0.05, which is in good agreement with the results obtained by Johnson et al. (2014).

8.3. The odd-Z elements: Na, Al, and K

Sodium abundances of bulge stars have been derived in Cunha06. Abundances of Na and Al in bulge stars are determined in Lecureur et al. (2007), Fulbright et al. (2007b), and Johnson et al. (2014). To our knowledge there is no previous determination of K in bulge stars. The odd-Z elements Na and Al are believed to be produced via a variety of processes (Smiljanic et al. 2016, and references therein), while K is thought to be mainly formed in Type II SNe (Samland 1998). Smiljanic et al. (2016) reports evidence that the surface abundance of Na varies according to the stellar evolution of giants, possibly making our sample of giant stars unsuitable for tracing the chemical evolution of this element in the
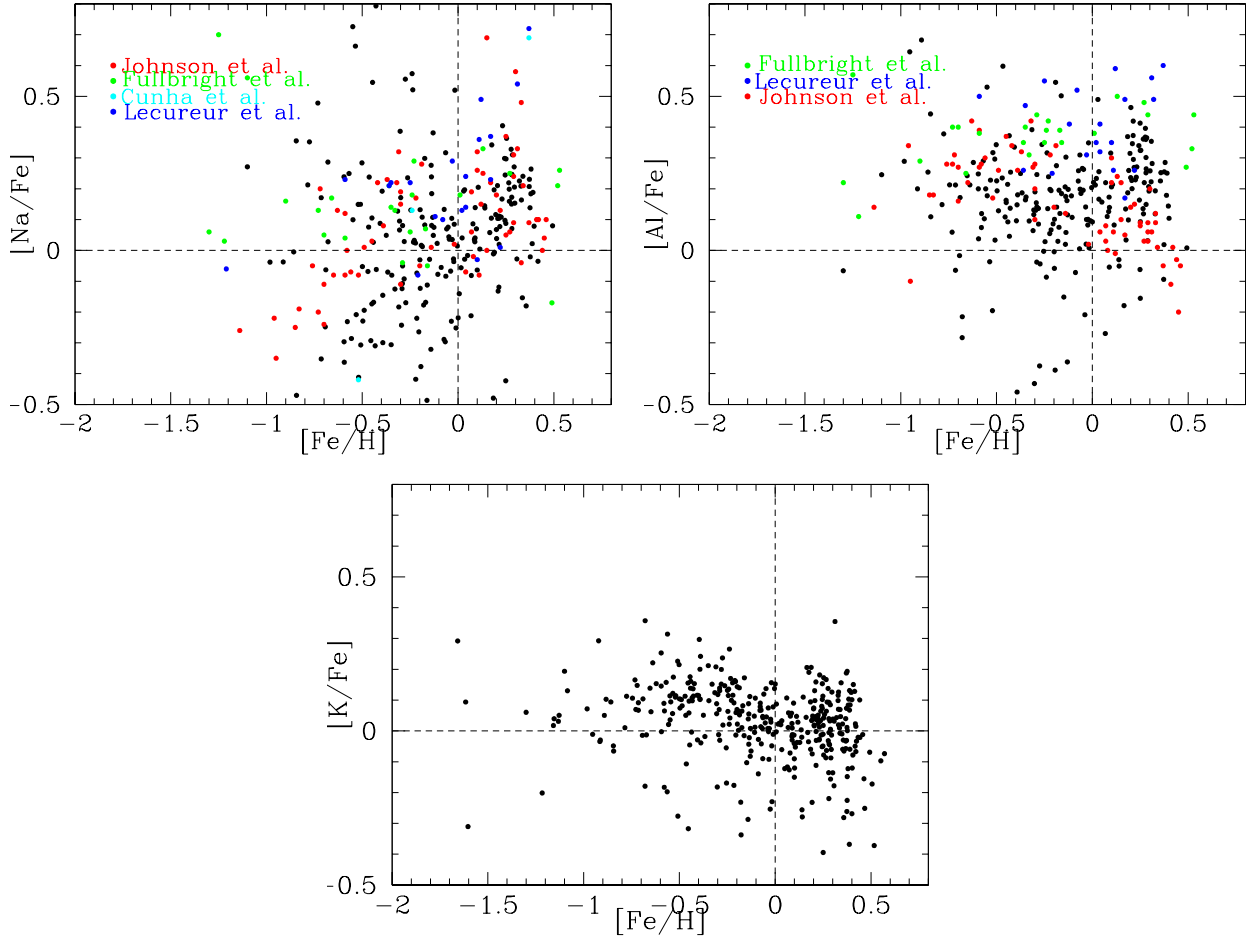
Fig. 15. [Fe/H] vs. [X/Fe] of APOGEE stars in BW for odd-Z elements compared with literature values.

bulge. Figure 15 suggests that compared to other bulge works using giants (Cunha06, Fulbright et al. 2007b; Lecureur et al. 2007; and Johnson et al. 2014), our results have larger scatter, but likely follow the same trend of rising [Na/Fe] for higher [Fe/H], as in Fulbright et al. (2007b), Lecureur et al. (2007), and Johnson et al. (2014).

Figure 15 also demonstrates that our results appear to corroborate the aluminium trend found in Johnson et al. (2014), albeit with a larger scatter. Lecureur et al. (2007) and Fulbright et al. (2007b), however, find – on average – higher values of [Al/Fe], especially at higher metallicities. McWilliam (2016) have shown that [Al/Fe] displays an alpha-like trend (see their Fig. 5), which is expected as Al production occurs in post carbon-burning hydrostatic phases of massive stars. A comparison of [Al/Fe] in the bulge, the Milky Way disc, and the Sgr dwarf galaxy suggests that the Al yields also depend on the progenitor metallicity (Fulbright et al. 2007b).

Our [K/Fe] vs. [Fe/H] trend shown in Fig. 15 observationally resembles an α-like trend, with decreasing [K/Fe] for increasing [Fe/H], similar to what APOGEE finds for the discs. However, the bulge [K/Fe]-values for the most metal-rich stars are higher than for the disc stars of corresponding metallicity.

In conclusion, we have shown that chemical abundances from APOGEE in BW (C, N, O, Na, Mg, Al, Si, K, Ca, Cr, Mn, Co, and Ni) follow in general a tight sequence in the [Fe/H] vs. [X/Fe] plane and agree well with known high-resolution abundance studies.

9. Summary

We have investigated the MDF for a large sample of stars in BW with APOGEE, and found a remarkable agreement with the MDF of GES; both exhibit a bimodal distribution. The ARGOS survey, in contrast, exhibits three distinguishable peaks. The reason for this difference could be the use of photometric temperatures using $(J-K)$ colours which could have effects on the MDF. In the [Mg/Fe] vs. [Fe/H] plane, APOGEE and GES exhibit very similar results, although for higher metallicities ([Fe/H] > +0.1) APOGEE exhibits higher abundance levels with respect to the GES. We used the [C/N] ratio to derive the age distribution for a subset of the stars in BW, following Martig et al. (2016), and found a bimodal distribution with a peak of ~10 Gyr and a significant fraction of young stars (~3−4 Gyr). Our findings are comparable with those of Bensby et al. (2013) and Haywood et al. (2016). However, more data are necessary to constrain the age distribution in BW.

We have compared stellar parameters and individual abundances for α- and iron-peak elements from the APOGEE pipeline (DR13) with known literature values for stars in BW. The difference between photometric $\log g$ values and spectroscopic determinations shows a strong linear relation with the spectroscopic $\log g$ of APOGEE. TRILEGAL simulations suggest that this effect is due to the intrinsic depth of the bulge, thus photometric surface gravities in the Galactic bulge should be treated with caution. Compared to the relatively small number of measurements in the literature, APOGEE traces heavy elements

covering a large metallicity range ($-1 <$ [Fe/H] $< +0.5$) in the bulge. In general, the comparison between individual abundances of O, Na, Mg, Al, Si, K, Ca, Cr, Mn, Co, and Ni from APOGEE with that of literature values shows an overall good agreement.

References

Allende Prieto, C., Beers, T. C., Wilhelm, R., et al. 2006, ApJ, 636, 804
Alonso, A., Arribas, S., & Martínez-Roger, C. 1999, A&AS, 140, 261
Alves-Brito, A., Meléndez, J., Asplund, M., Ramírez, I., & Yong, D. 2010, A&A, 513, A35
Arp, H. 1965, ApJ, 141, 43
Babusiaux, C., Gómez, A., Hill, V., et al. 2010, A&A, 519, A77
Barbuy, B., Hill, V., Zoccali, M., et al. 2013, A&A, 559, A5
Battistini, C., & Bensby, T. 2015, A&A, 577, A9
Bensby, T., Yee, J. C., Feltzing, S., et al. 2013, A&A, 549, A147
Borucki, W. J., Koch, D., Basri, G., et al. 2010, Science, 327, 977
Bravo, E., & Martínez-Pinedo, G. 2012, Phys. Rev. C, 85, 055805
Bressan, A., Marigo, P., Girardi, L., et al. 2012, MNRAS, 427, 127
Chatzopoulos, S., Fritz, T. K., Gerhard, O., et al. 2015, MNRAS, 447, 948
Church, R. P., Johnson, J. A., & Feltzing, S. 2011, A&A, 529, A104
Clarkson, W., Sahu, K., Anderson, J., et al. 2008, ApJ, 684, 1110
Cunha, K., & Smith, V. V. 2006, ApJ, 651, 491
Eisenstein, D. J., Weinberg, D. H., Agol, E., et al. 2011, AJ, 142, 72
Freeman, K., Ness, M., Wylie-de-Boer, E., et al. 2013, MNRAS, 428, 3660
Fulbright, J. P., McWilliam, A., & Rich, R. M. 2006, ApJ, 636, 821
Fulbright, J. P., McWilliam, A., & Rich, R. M. 2007a, ApJ, 661, 1152
Fulbright, J. P., McWilliam, A., & Rich, R. M. 2007b, ApJ, 661, 1152
García Pérez, A. E., Allende Prieto, C., Holtzman, J. A., et al. 2016, AJ, 151, 144
Gilmore, G., Randich, S., Asplund, M., et al. 2012, The Messenger, 147, 25
Girardi, L., Barbieri, M., Groenewegen, M. A. T., et al. 2012, Astrophysics and Space Science Proceedings, 26, 165
Gonzalez, O. A., Rejkuba, M., Zoccali, M., et al. 2011a, A&A, 530, A54
Gonzalez, O. A., Rejkuba, M., Zoccali, M., Valenti, E., & Minniti, D. 2011b, A&A, 534, A3
Gonzalez, O. A., Rejkuba, M., Zoccali, M., et al. 2012, A&A, 543, A13
Gonzalez, O. A., Zoccali, M., Vasquez, S., et al. 2015, A&A, 584, A46
González Hernández, J. I., & Bonifacio, P. 2009, A&A, 497, 497
Gunn, J. E., Siegmund, W. A., Mannery, E. J., et al. 2006, AJ, 131, 2332
Hawkins, K., Masseron, T., Jofré, P., et al. 2016, A&A, 594, A43
Hayden, M. R., Bovy, J., Holtzman, J. A., et al. 2015, ApJ, 808, 132
Haywood, M., Di Matteo, P., Snaith, O., & Calamida, A. 2016, A&A, 593, A82
Hill, V., Lecureur, A., Gómez, A., et al. 2011, A&A, 534, A80
Holtzman, J. A., Shetrone, M., Johnson, J. A., et al. 2015, AJ, 150, 148
Johnson, C. I., Rich, R. M., Kobayashi, C., Kunder, A., & Koch, A. 2014, AJ, 148, 67
Jönsson, H., Ryde, N., Schultheis, M., & Zoccali, M. 2017, A&A, 598, A101
Kobayashi, C., Umeda, H., Nomoto, K., Tominaga, N., & Ohkubo, T. 2006, ApJ, 653, 1145
Lecureur, A., Hill, V., Zoccali, M., et al. 2007, A&A, 465, 799
Majewski, S. R., Schiavon, R. P., Frinchaboy, P. M., et al. 2015, AJ, submitted [arXiv:1509.05420]
Martig, M., Fouesneau, M., Rix, H.-W., et al. 2016, MNRAS, 456, 3655
Matteucci, F., & Brocato, E. 1990, ApJ, 365, 539
McWilliam, A. 2016, PASA, 33, e040
McWilliam, A., & Rich, R. M. 1994, ApJS, 91, 749
McWilliam, A., Rich, R. M., & Smecker-Hane, T. A. 2003, ApJ, 592, L21
Meléndez, J., Asplund, M., Alves-Brito, A., et al. 2008, A&A, 484, L21
Mikolaitis, Š., Hill, V., Recio-Blanco, A., et al. 2014, A&A, 572, A33
Ness, M., Freeman, K., Athanassoula, E., et al. 2013, MNRAS, 430, 836
Nishiyama, S., Tamura, M., Hatano, H., et al. 2009, ApJ, 696, 1407
Nissen, P. E., Chen, Y. Q., Schuster, W. J., & Zhao, G. 2000, A&A, 353, 722
Pasquini, L., Alonso, J., Avila, G., et al. 2003, in Instrument Design and Performance for Optical/Infrared Ground-based Telescopes, eds. M. Iye, & A. F. M. Moorwood, Proc. SPIE, 4841, 1682
Prochaska, J. X., Naumov, S. O., Carney, B. W., McWilliam, A., & Wolfe, A. M. 2000, AJ, 120, 2513
Recio-Blanco, A., de Laverny, P., Allende Prieto, C., et al. 2016, A&A, 585, A93
Recio-Blanco, A., Rojas-Arriagada, A., de Laverny, P., et al. 2017, A&A, accepted [arXiv:1702.04500]
Rich, R. M. 1988, AJ, 95, 828
Rich, R. M., & Origlia, L. 2005, ApJ, 634, 1293
Rojas-Arriagada, A., Recio-Blanco, A., Hill, V., et al. 2014, A&A, 569, A103
Rojas-Arriagada, A., Recio-Blanco, A., de Laverny, P., et al. 2017, A&A, submitted
Ryde, N., Gustafsson, B., Edvardsson, B., et al. 2010, A&A, 509, A20
Sadler, E. M., Rich, R. M., & Terndrup, D. M. 1996, AJ, 112, 171
Samland, M. 1998, ApJ, 496, 155
Santiago, B. X., Brauer, D. E., Anders, F., et al. 2016, A&A, 585, A42
SDSS Collaboration, Albareti, F. D., Allende Prieto, C., et al. 2016, ApJS, submitted [arXiv:1608.02013]
Smiljanic, R., Romano, D., Bragaglia, A., et al. 2016, A&A, 589, A115
Stanek, K. Z. 1996, ApJ, 460, L37
Uttenthaler, S., Schultheis, M., Nataf, D. M., et al. 2012, A&A, 546, A57
Valenti, E., Zoccali, M., Renzini, A., et al. 2013, A&A, 559, A98
Woosley, S. E., & Weaver, T. A. 1995, ApJS, 101, 181
Zamora, O., García-Hernández, D. A., Allende Prieto, C., et al. 2015, AJ, 149, 181
Zasowski, G., Johnson, J. A., Frinchaboy, P. M., et al. 2013, AJ, 146, 81
Zoccali, M., Renzini, A., Ortolani, S., et al. 2003, A&A, 399, 931
Zoccali, M., Lecureur, A., Barbuy, B., et al. 2006, A&A, 457, L1
Zoccali, M., Hill, V., Lecureur, A., et al. 2008, A&A, 486, 177
Zoccali, M., Vasquez, S., Gonzalez, O. A., et al. 2017, A&A, 599, A12